Combustion and exhaust emission characteristics, and in-cylinder gas composition, of hydrogen enriched biogas mixtures in a diesel engine

Midhat Talibi[*], Paul Hellier, Nicos Ladommatos

Department of Mechanical Engineering, University College London, Torrington Place, London, WC1E 7JE, United Kingdom

ARTICLE INFO

ABSTRACT

This paper presents a study undertaken on a naturally aspirated, direct injection diesel engine investigating the combustion and emission characteristics of CH_4-CO_2 and CH_4-CO_2-H_2 mixtures. These aspirated gas mixtures were pilot-ignited by diesel fuel, while the engine load was varied between 0 and 7 bar IMEP by only adjusting the flow rate of the aspirated mixtures. The in-cylinder gas composition was also investigated when combusting CH_4-CO_2 and CH_4-CO_2-H_2 mixtures at different engine loads, with in-cylinder samples collected using two different sampling arrangements.

The results showed a longer ignition delay period and lower peak heat release rates when the proportion of CO_2 was increased in the aspirated mixture. Exhaust CO_2 emissions were observed to be higher for $60CH_4$:$40CO_2$ mixture, but lower for the $80CH_4$:$20CO_2$ mixture as compared to diesel fuel only combustion at all engine loads. Both exhaust and in-cylinder NOx levels were observed to decrease when the proportion of CO_2 was increased; NOx levels increased when the proportion of H_2 was increased in the aspirated mixture. In-cylinder NOx levels were observed to be higher in the region between the sprays as compared to within the spray core, attributable to higher gas temperatures reached, post ignition, in that region.

© 2017 The Authors. Published by Elsevier Ltd. This is an open access article under the CC BY license (http://creativecommons.org/licenses/by/4.0/).

1. Introduction

Biogas, produced via anaerobic digestion of organic matter, is considered to be a carbon-neutral fuel since the carbon emitted when burning biogas comes from plant matter that fixed this carbon from atmospheric carbon dioxide (via the natural carbon cycle). The primary component of biogas is methane (50—80% by volume depending on the method of biogas production), which is a greenhouse gas (GHG) with a global warming factor about 20 times higher than CO_2; burning biogas converts the CH_4 to CO_2, thereby reducing the GHG impact on the environment. Therefore, since biogas production involves capturing CH_4 produced during decomposition of organic waste products (that would otherwise degrade in an open environment), utilization of biogas reduces direct emissions of CH_4 to the atmosphere [1,2].

Biogas has a relatively high octane number of about 130 (due to the presence of CH_4), thereby exhibiting greater resistance to phenomena such as knock, and making it appropriate for use in CI engines which typically have high compression ratios [3,4]. However, biogas has an autoignition temperature of 1087 K [1], and since the air temperature reached at the end of the compression stroke in a CI engine is typically about 800 K, liquid fuel is required to ignite the biogas in a diesel engine. Additionally, since biogas has a lower carbon content compared to conventional diesel fuel, the use of biogas as the primary fuel, with only a small amount of pilot diesel fuel, results in significantly lower carbon pollutant emissions (CO_2 and particulates). Consequently, this also allows burning very lean or diluted biogas and air mixtures, resulting in low temperature combustion, and hence reduced NO_x emissions. Therefore biogas-diesel fuel co-combustion is well suited for CI engines and has both economical (with biogas produced from organic waste) and environmental benefits, providing low pollutant emission combustion while still maintaining diesel fuel comparable efficiencies [1,5].

There have been many studies conducted in the past investigating the utilization of biogas in CI engines, in addition to studying the combustion characteristics of biogas obtained from various feedstock [1,6—11]. Bari [8] studied the effect of CO_2 concentration in a biogas fuelled diesel engine. An increase in BSFC was reported for CO_2 concentrations above 20—30% by volume in the biogas. This

was attributed to CO_2 being a diluent in the combustion chamber, absorbing energy from the combustion flame, lowering local gas temperatures and affecting the burning velocity of the biogas-air mixture. However, a slight decrease in BSFC was seen below 20% CO_2 concentration, which was speculated to have been due to oxygen radicals, released via dissociation of CO_2, reducing ignition delay and enhancing carbon oxidation. Henham & Makkar [12] undertook similar tests, making use of simulated biogas to represent the varying CH_4:CO_2 ratios of biogas available from different sources. The effect of CH_4 proportion in biogas and of the quantity of pilot fuel was studied on a two-cylinder diesel engine, over a range of engine speeds and loads. The results indicated that 60% substitution of diesel fuel with biogas could be achieved without the occurrence of knock, however, the engine thermal efficiency was observed to decrease as diesel fuel was increasingly replaced with biogas.

Other investigations have also examined the effect of biogas-diesel co-combustion on exhaust gas emissions. Bedoya et al. [9] tested the performance of a DI diesel engine with simulated biogas (60% CH_4 - 40% CO_2), utilising a supercharger and a Kenics mixer system in the intake. The authors reported that the supercharged mixing system allowed almost complete diesel substitution by biogas (except for a small quantity of pilot fuel), increased thermal efficiency, and reduced CH_4 and CO exhaust gas emissions. Yoon & Lee [5] carried out an experimental investigation comparing the combustion and emission characteristics of an engine operating on diesel fuel only and biogas-fossil diesel mixtures (dual fuel mode). An increase in ignition delay was observed for the dual fuel mixtures, as compared to diesel fuel only engine operation. This was attributed to the relatively low charge temperatures of the biogas-air mixture and high specific heat capacity of the biogas; the exhaust gas temperatures for the dual fuel engine operation were found to be lower than single fuel modes attributable to the same reason. Both NO_x and particulate emissions were lower under dual fuel operation as compared to diesel only mode; the low NO_x emissions were attributed to the reduced in-cylinder gas temperatures, whereas the reduction in soot emissions was suggested to be due to the lower carbon content of biogas relative to fossil diesel. However, a significant increase in HC and CO emissions was observed when running the engine in dual fuel mode, with the increase in HC attributed to unburned biogas in the combustion chamber persisting to the exhaust. Mustafi et al. [13] carried out a comparative study between biogas and natural gas fuelled engines and reported a 12% reduction in NO_x and a 70% reduction in PM mass emissions for the natural gas-diesel operation relative to diesel only combustion. Although unburned HC emissions increased in the case of both the gaseous fuels, the HC emissions were higher for biogas fuelling due to the presence of CO_2. An increase in BSFC and in the duration of ignition delay was observed when biogas was introduced to the engine; these increases in BSFC and ignition delay were found to be proportionate to the amount of CO_2 present in the exhaust gas.

The increase in ignition delay observed when fuelling CI engines with biogas-diesel fuel mixtures is disadvantageous as it results in higher premixed combustion and peak heat rates, leading to a reduction in engine efficiency, increase in exhaust NO_x emission levels and a possibility of causing damage to mechanical parts of the engine [14—16]. The ignition delay increases due to displacement of intake air O_2 by the aspirated biogas, resulting in lower effective temperatures during compression and a reduced quantity of reactive radicals available at the time of autoignition. Cacua et al. [17] tried to overcome this problem, when co-combusting biogas-diesel fuel mixtures, by increasing the O_2 concentration in the intake air up to 27% by volume. A reduction in ignition delay was observed at all O_2 enrichment levels due to the higher amount of O_2

available during the ignition process. At the highest level of O_2 enrichment and a 40% engine load condition, a 28% increase in thermal efficiency was observed (relative to non-enriched air), attributed to the increased rate of fuel oxidation reactions and high flame propagation velocities. A considerable decrease in the exhaust emissions of methane and CO were also reported for all levels of O_2 enrichment.

The above review of literature suggests that while the co-combustion of biogas with diesel fuel has the potential of providing low pollutant emission combustion, the presence of CO_2 in the biogas tends to increase ignition delay periods and reduce flame propagation speeds resulting in a drop in engine thermal efficiencies. One potential way of countering this, without having an adverse effect on emission levels, is to add hydrogen (H_2) to the biogas mixture. The flame speed of H_2 (230 cm/s) is approximately six times higher than that of CH_4 (42 cm/s) at atmospheric conditions [18,19]. This allows a shorter interval between fuel ignition and peak heat release, and therefore higher peak cylinder pressures and heat release rates, closer to engine TDC. The thermal energy absorbing effects of the inert CO_2 in biogas during combustion could be countered by the addition of H_2. However, previous studies of H_2-diesel co-combustion [20—22] have reported significant increase in NO_x emissions at high H_2 addition levels. The use of biogas with H_2 could possibly reduce in-cylinder gas temperatures, hence reducing NO_x emissions. The current study attempts to understand the combustion and emission characteristics of hydrogen enriched biogas fuelled diesel engines, and consider any synergy between biogas, hydrogen and diesel fuel co-combustion.

The study reported in the current paper presents experimental results from the combustion of different CH_4-CO_2 and CH_4-CO_2-H_2 mixtures, pilot ignited by two different diesel fuel flow rates. Additionally, samples were collected from within the engine cylinder to provide validation for the exhaust emission results and to analyse the variations in in-cylinder gas composition at different stages of the engine cycle, when combusting CH_4-CO_2 and CH_4-CO_2-H_2 mixtures. Finally, some exhaust emission tests were conducted with actual biogas samples obtained from an anaerobic digester, which used animal manure as organic waste to produce biogas.

2. Experimental setup

2.1. Engine facility

The experiments described in this study were carried out on a single cylinder CI engine which has been described in detail previously by the author [22]. The engine comprises of a cylinder head, piston and connecting rod from a 2.0 L 4-cylinder Ford Duratorq donor engine, installed on a single cylinder Ricardo Hydra crankcase; Table 1 lists the geometry specifications for the engine. The

Table 1
Engine specifications.

Bore	86 mm
Stroke	86 mm
Swept volume	499.56 cm³
Compression ratio (geometric)	18.3: 1
Maximum in-cylinder pressure	150 bar
Piston design	Central ω − bowl in piston
Fuel injection pump	Delphi single-cam radial-piston pump
High pressure common rail	Delphi solenoid controlled, 1600 bar max.
Diesel fuel injector	Delphi DFI 1.3 6-hole solenoid valve
Electronic fuel injection system	1 µs duration control
Crank shaft encoder	1800 ppr, 0.2 CAD resolution
Oil and coolant temperature	80 ± 2.5 °C

in-cylinder gas pressure was measured to a resolution of 0.2 CAD using a Kistler 6056A piezoelectric pressure transducer and a Kistler 5018 charge amplifier. The operation pressure and temperature readings were logged using PCs in conjunction with National Instruments (NI) data acquisition systems. An in-house developed NI LabVIEW program evaluated the in-cylinder pressure data in real-time to determine net apparent heat release rates and the indicated mean effective pressure (IMEP).

The intake air flow rate was measured using a positive displacement volumetric air flow meter (Romet G65), while the flow of CH_4, CO_2 and H_2 into the engine intake was metered precisely using Bronkhorst thermal mass flow controllers to an accuracy of 0.05 l/min. The CH_4, CO_2 and H_2 were supplied from compressed gas bottles and fed into the engine inlet manifold 350 mm upstream of the inlet valves. A Delphi DFI 1.3 six-hole, servo-hydraulic solenoid valve fuel injector was used to inject diesel fuel directly into the combustion chamber with an EmTronix EC-GEN 500 engine system used to control the injection pressure, injection timing and duration of injection.

The exhaust gases were sampled 30 mm downstream of the engine exhaust valves and conveyed to the analysers via heated lines maintained at 190 °C and 80 °C for the measurement of gaseous and particulate emissions respectively. The gaseous exhaust emissions were sampled by a Horiba analyser rack (MEXA-9100HEGR) which measured the volumetric concentration of CO, CO_2, unburned THC, NO_x and O_2 in the gas sample. A differential mobility spectrometer (Cambustion DMS500) was utilised to determine the exhaust particulate mass and size distribution.

Fig. 1 shows a schematic of the experimental setup, including gas delivery and exhaust measurement systems.

2.2. In-cylinder gas sampling system

An in-house developed sampling system, described in Talibi et al. [23], was used to collect engine in-cylinder gas samples at various stages during the engine cycle. The sampling system consisted of an electromagnetically actuated sampling valve (Fig. 2) and a heated dilution tunnel. The electromagnetic armature of the sampling valve was not connected directly to the valve stem ('percussion' principle) which allowed shorter sampling durations (<1 ms). When current was supplied to the electromagnetic armature, it accelerated and travelled at high speeds towards the valve stem impacting it with a force large enough to open the poppet valve very briefly (for about 6—10 CAD), allowing a small gas

Fig. 1. Schematic showing test engine arrangement including gas mixture delivery and exhaust emissions instrumentation.

sample to be collected from the engine cylinder. A sensitive proximity sensor, installed so as to sense the displacement of the stem of the sampling valve, continuously monitored the poppet valve lift (of order 0—0.5 mm). The timing controller for the sampling valve was synchronised with the engine crankshaft encoder, allowing the valve to be opened at any desired crank angle in the engine cycle, to a resolution of 0.2 CAD. The sampling valve was installed in the cylinder head replacing one of the two engine intake valves, with the sampling valve tip able to penetrate up to 9 mm into the combustion chamber. Fig. 3 shows the position of the sampling valve in the cylinder head relative to the diesel fuel injector and piston position at TDC.

The gas samples extracted by the sampling valve were fed into the heated dilution tunnel which was maintained at 200 °C. The purpose of the tunnel was to buffer the gas samples and mix them with heated nitrogen gas (at 180 °C) to increase the volume of the sample sufficiently so that it could be measured by the Horiba emissions analyser (which required a sample flow rate of at least 30 l/min). The undiluted and diluted gas sample streams were consecutively fed into a stand-alone CO_2 analyser (which functioned with relatively lower flow rates) and to the Horiba emissions analyser respectively. The mass ratio of the undiluted to the diluted in-cylinder gas sample was calculated by means of measured molar concentrations of CO_2 by the analysers in the undiluted and diluted gas sample. The sample gas composition measured by the analysers was assumed to be representative of the average concentration of stable species in the combustion chamber that were extracted during the short sampling window. This is because it is expected that the high rates of heat transfer from the gas sample to the valve seat, combined with the expansion of the sample gas from cylinder gas pressure (40—100 bar) to near atmospheric pressure, causes the sample gas temperature to drop rapidly, quenching any combustion reactions.

3. Experimental procedure and test fuels

All the tests described in this paper were carried out at a constant engine speed of 1200 rpm, common rail fuel injection pressure of 900 bar and a diesel fuel injection timing of 10 CAD BTDC. A speed of 1200 rpm was selected as it allowed a better sampling resolution (that is, sampling over fewer crank angle degrees) when using the in-cylinder sampling system. A speed of lower that 1200 rpm would have meant sampling over more crank angle degrees (larger sampling windows). A higher engine speed caused unstable valve operation due to shorter time available for sampling valve O-rings to decompress. The diesel injector had been previously calibrated at engine steady-state, and the volumetric flow rate of diesel fuel through the injector could be determined at different diesel fuel injection duration periods using calibration curves. The diesel fuel used was of fossil origin, with zero fatty acid methyl ester (FAME) content, cetane number of 53.2 and carbon to hydrogen ratio of 6.32:1 by mass. Compressed CH_4 gas of purity 99.5%, and compressed H_2 and compressed CO_2 gases, each of purity 99.995%, were obtained from a commercial gas supplier (BOC).

3.1. Experimental set 1: exhaust emission tests (using CH_4-CO_2-H_2 mixtures)

The test procedure followed for these set of tests consisted of fixing the diesel fuel flow rate supplied to the engine, while gradually increasing the amount of CH_4-CO_2-H_2 mixture being delivered to the engine so as to increase the engine load (power output measured in bar IMEP), at constant engine speed. The fossil diesel fuel contributed a small fraction of the total fuel energy supplied to the engine which was primarily utilised to pilot-ignite the gaseous
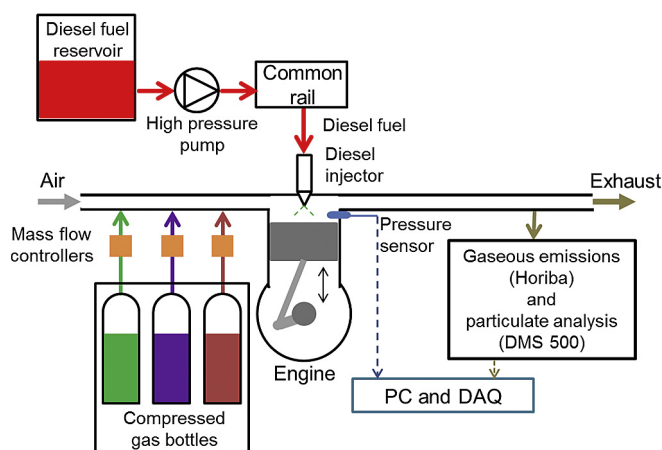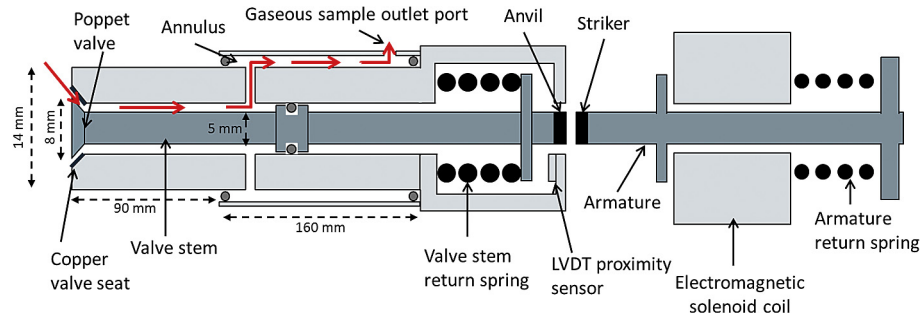
Fig. 2. Simplified diagram of the in-cylinder sampling valve showing the gas flow (red arrows) from within the cylinder to the sample outlet port. (For interpretation of the references to colour in this figure legend, the reader is referred to the web version of this article.)
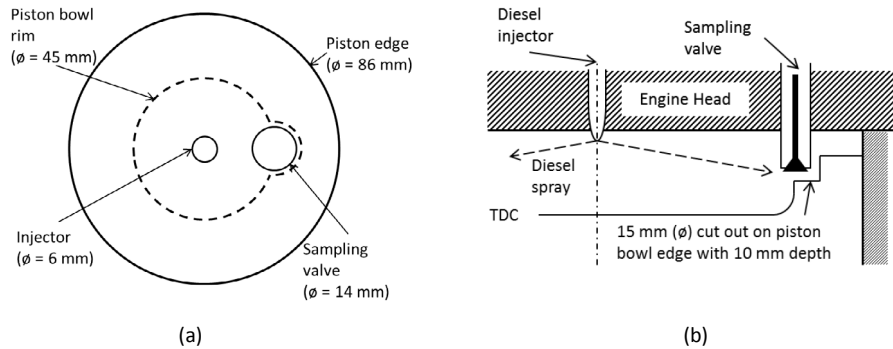

(a)   (b)

Fig. 3. Schematic showing (a) plan view and (b) cross-sectional side view of the relative locations of the injector, the sampling valve at maximum in-cylinder penetration and the piston at TDC.

CH_4-CO_2-H_2 mixture. The engine output developed by the fixed diesel fuel flow is henceforth referred to as the pilot diesel fuel IMEP in this paper. Two series of tests were conducted with two different pilot diesel fuel flow rates, which were sufficient to develop engine loads of 0 bar and 1.5 bar, respectively, on their own. For a pilot diesel fuel only IMEP of 0 bar without supply of the gaseous mixture, no heat release could be discerned from the analysis of in-cylinder gas pressure, however, reliable ignition of the aspirated gaseous mixture was achieved at all engine loads. It is therefore assumed that at the diesel flow rate, equivalent to a pilot diesel fuel IMEP of 0 bar, was the minimum flow rate at which diesel spray released from the fuel injector nozzle at sufficient quantities to not only self-ignite but also cause ignition the aspirated CH_4-CO_2-H_2 mixture at all engine loads up to 7 bar IMEP.

Each of the two pilot diesel IMEPs 0 and 1.5 bar were co-combusted with different CH_4-CO_2 and CH_4-CO_2-H_2 mixtures (henceforth, collectively termed as CH_4-CO_2-H_2 mixtures), as detailed in Table 2. The two CH_4-CO_2 mixtures tested, $60CH_4$:$40CO_2$ (v/v) and $80CH_4$:$20CO_2$ (v/v), represent typical biogas qualities: biogas which has been obtained directly from anaerobic digesters and biogas which has undergone post-production CO_2 scrubbing, respectively. H_2 was added in molar proportions of 5% and 15% to the CH_4-CO_2 mixture; the relative proportions of CH_4 and CO_2 were kept constant at all H_2 addition levels. Table 3 shows the salient properties of the fuels and gases utilised in these experiments. Fig. 4 shows the energy supplied to the engine from the different CH_4-CO_2-H_2 mixtures as a function of the total energy supplied to the engine (energy from the CH_4-CO_2-H_2 mixtures plus diesel), for the two pilot diesel fuel IMEPs of 0 bar and 1.5 bar.

An additional series of baseline (control) tests were carried out, for comparison, using diesel fuel only (without any CH_4-CO_2-H_2 mixture addition), with the diesel fuel injection period (and hence

the diesel fuel flow rate delivered to the engine) gradually increased so that the engine load increased from 0 to 7 bar IMEP.

3.2. Experimental set 2: in-cylinder gas sampling tests (using CH_4-CO_2-H_2 mixtures)

A further set of experiments was carried out utilising the in-cylinder gas sampling system installed on the single cylinder engine; for these experiments the diesel fuel flow rate was also fixed so as to provide a constant pilot diesel fuel IMEP of 1.5 bar. At this engine load of 1.5 bar IMEP, and with no CH_4, CO_2 or H_2 supplied to the engine, only negligible levels of NO_x were measured in the exhaust gases. Therefore, in the course of the in-cylinder sampling experiments, it would be reasonable to assume that any observed NO_x could primarily be attributed to the presence of CH_4-CO_2-H_2 mixtures generating NO_x on their own account or in synergy with the diesel fuel. It is worth noting that at the engine load of 1.5 bar IMEP sufficient fossil diesel fuel was supplied to the engine for the development of measurable heat release from diesel only combustion.

These tests were conducted at engine loads of 3, 4, 5 and 5.5 bar IMEP by supplying the necessary amount of CH_4-CO_2-H_2 mixture to the engine to increase the engine load beyond the 1.5 bar IMEP provided by the pilot diesel fuel. The engine was supplied with $60CH_4$:$40CO_2$ (v/v) and $60CH_4$:$40CO_2$ + 15% H_2 (v/v) mixtures and the composition of in-cylinder combustion gases investigated.

During these tests, gas samples were extracted from the engine cylinder utilising two distinct sampling arrangements, relative to one of the six injector nozzle diesel fuel sprays (Fig. 5) With the first arrangement (Fig. 5a), in-cylinder samples were collected from a region of high diesel fuel concentration within the core of the diesel fuel spray, while with the second arrangement (Fig. 5b), samples

Table 2
Test parameter matrix for the exhaust emission experiments.

Pilot diesel (bar IMEP)	Diesel fuel flow rate (ml/min)	Aspirated mixture ratio (v/v)	$CH_4:CO_2:H_2$ mixture ratio (v/v)	CH_4 flow rate (l/min)	CO_2 flow rate (l/min)	H_2 flow rate (l/min)	Engine IMEP (bar)
0	1.40	$60CH_4:40CO_2$	60:40:0	8.5—13.7	5.7—9.1	0	0—7
		95% ($60CH_4:40CO_2$) + 5% H_2	57:38:5	8.1—13.1	5.4—8.8	0.7—1.2	
		85% ($60CH_4:40CO_2$) + 15% H_2	51:34:15	7.2—12.2	4.8—8.1	2.1—3.6	
		$80CH_4:20CO_2$	80:20:0	8.0—13.0	2.0—3.3	0	
		95% ($80CH_4:20CO_2$) + 5% H_2	76:19:5	7.6—12.6	1.9—3.2	0.5—0.8	
		85% ($80CH_4:20CO_2$) + 15% H_2	68:17:15	7.1—12.2	1.8—3.0	1.6—2.7	
1.5	3.65	$60CH_4:40CO_2$	60:40:0	1.6—11.1	1.1—7.4	0	1.5—7
		95% ($60CH_4:40CO_2$) + 5% H_2	57:38:5	1.7—10.5	1.1—7.0	0.5—0.9	
		85% ($60CH_4:40CO_2$) + 15% H_2	51:34:15	1.6—10.0	1.1—6.6	0.5—2.9	
		$80CH_4:20CO_2$	80:20:0	4.0—10.2	1.0—2.5	0	
		95% ($80CH_4:20CO_2$) + 5% H_2	76:19:5	6.1—10.6	1.5—2.7	0.4—0.7	
		85% ($80CH_4:20CO_2$) + 15% H_2	68:17:15	4.1—9.3	1.0—2.5	0.9—2.2	

Table 3
Lower heating value and density of diesel fuel, CH_4, CO_2 and H_2 at 1 atm and 300 K [18,24].

Fuel/gas	Lower heating value (MJ/m^3)	Density (kg/m^3)
Diesel fuel	36000	834.7
Methane (CH_4)	33	0.66
Carbon dioxide (CO_2)	—	1.91
Hydrogen (H_2)	10.05	0.084

were collected from an area of relatively low diesel fuel concentration between two fuel spray cones. Since the absolute location of the sampling valve in the engine head was fixed, the change in the sampling arrangement was achieved through rotation of the centrally-located injector. The approximate locations of the diesel fuel spray plumes were experimentally determined beforehand by rotating the diesel fuel injector in small angle steps and measuring the in-cylinder gas composition (in particular the levels of
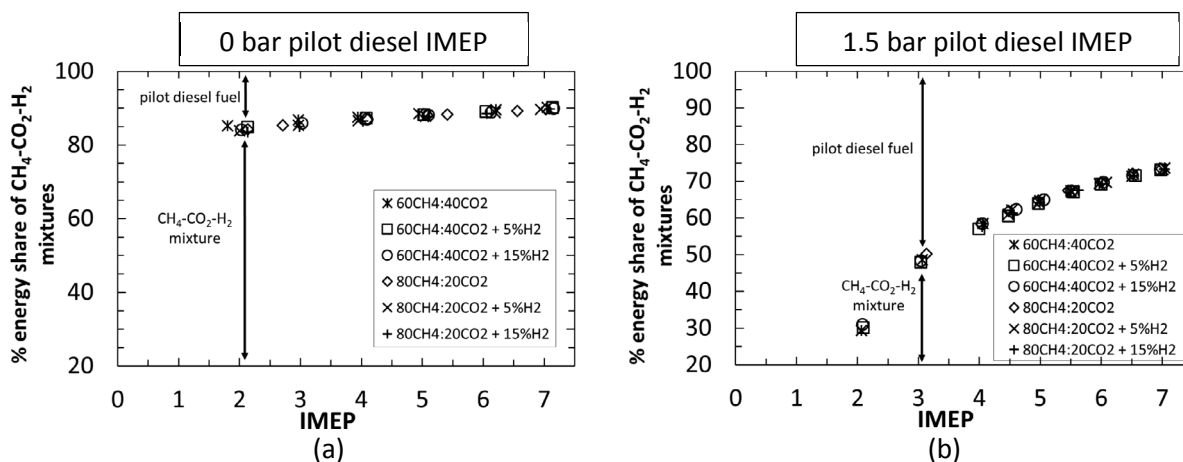

Fig. 4. Percentage energy supplied to the engine from the different CH_4-CO_2 and CH_4-CO_2-H_2 mixtures for (a) 0 bar and (b) 1.5 bar pilot diesel IMEP, at various engine loads (IMEP).
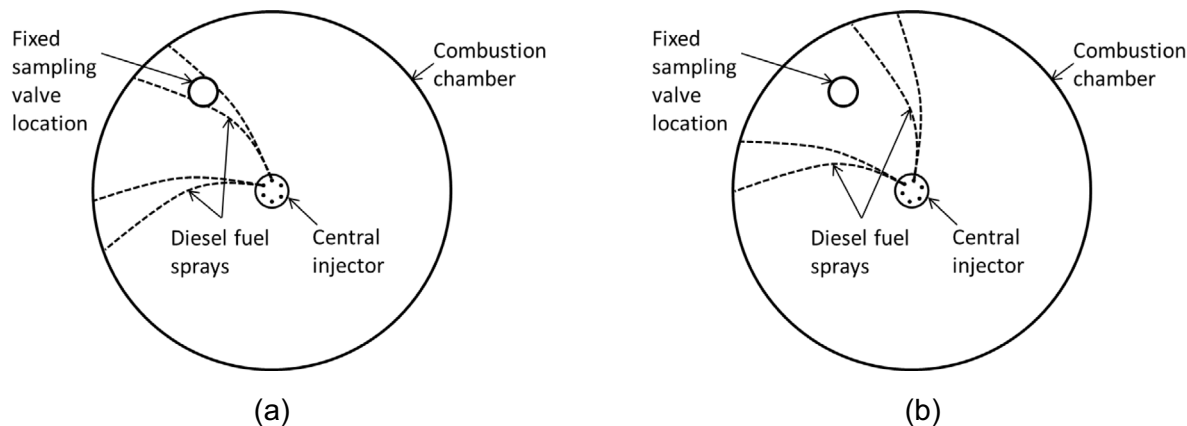

Fig. 5. Schematic showing (a) sampling arrangement one and (b) sampling arrangement two relative to the diesel fuel spray plumes; changes to the position of the plume relative to the valve location was achieved by rotating the fuel injector.

Table 4
In-cylinder gas sample extraction timings in CAD ATDC during the engine cycle and the corresponding sampling windows in CAD.

Sampling timing (middle of sampling window) (CAD ATDC)	Duration of sampling window (CAD)
10	6
25	10
40	15

unburned hydrocarbons) at each injector rotation angle. This methodology allowed approximate spray plume boundaries to be sketched, as indicated by the broken lines shown in Fig. 5.

For each of the two relative sampling arrangements, the extraction of gas samples was centred at three sampling windows in the engine cycle as follows: (a) during the premixed stage of combustion at 10 CAD ATDC; (b) during the early diffusion combustion stage at 25 CAD ATDC; and (c) during the late burning stage at 40 CAD ATDC. Table 4 lists the sampling valve crank angle timings and the sampling durations, within the engine cycle. It can be seen from Table 4 that the duration of the sampling window increased as the engine cycle progressed, attributable to decaying in-cylinder gas pressure. At lower in-cylinder gas pressures the flow rate through the valve sampling valve opening decreases quite rapidly. Hence, in order to obtain a sufficient volume flow rate of gas sample, in order to operate the analysers reliably, the valve had to be kept open for a longer duration.

3.3. Experimental set 3: exhaust emissions from real biogas

An additional set of tests were carried out using real biogas samples obtained from a commercial anaerobic digester operated on an urban farm within London, UK. The pre-fabricated bio-digester was a continuous flow reactor designed for small and medium sized farms, and converted organic waste, such as animal manure, into biogas (Fig. 6).

Two different samples of real biogas were tested with measured compositions of $54CH_4:40.5CO_2$ and $48CH_4:29CO_2$, with the balance assumed to be made up of inert components and common biogas contaminants such as hydrogen sulphide-H_2S (Table 5). The biogas was collected in Tedlar bags, and delivered to the engine via a positive displacement gas pump, at a constant flow rate of 4.6 l/min, which was the maximum achievable flow rate with the available gas pump. The engine load was varied by changing the diesel fuel injection period (and hence the diesel fuel flow rate delivered to the engine) to vary the engine load between 3 and 7 bar IMEP. These tests were of short durations since the H_2S in real biogas is known to cause damage to seals in the engine. Additionally, experiments were undertaken by the supplying the engine with simulated biogas of the same CH_4-CO_2 ratio as the real biogas in order to the compare exhaust emissions between the real and simulated biogas and investigate the effect of contaminants in the real biogas.

4. Results and discussion

4.1. Combustion characteristics

Fig. 7 shows the heat release rate curves for a pilot diesel fuel IMEP of 0 bar and supplying the engine with different CH_4-CO_2-H_2 mixtures, to achieve the required engine load of 4 bar IMEP. The graph also shows the heat release rate curve at the same engine load of 4 bar IMEP when the engine is operating on only diesel fuel. First, comparing the heat release rate curve of diesel only engine operation with that of diesel fuel pilot ignited CH_4-CO_2-H_2

mixtures, it can be observed that the rate of increase of heat release post ignition is considerably faster in the case of only diesel fuel, resulting in higher peak heat release rates closer to engine TDC. For diesel only combustion, an appreciable amount of diesel fuel-air mixture, prepared during the ignition delay period, is available for combustion which ignites and burns very rapidly. On the other hand, the pilot-ignited CH_4-CO_2-H_2 premixed mixtures are significantly leaner ($\varphi_{H2} = 0.018$ and $\varphi_{CH4} = 0.36$ for $80CH_4:20CO_2+15\%$ H_2 mixture at a total engine load of 4 bar IMEP), and hence they develop multiple flame fronts travel at considerably lower velocities than achievable with diesel only, premixed stoichiometric combustion. This results in slower rates of energy release, with lower peak heat release rates occurring further away from TDC and with longer combustion durations (Fig. 7). Another interesting feature to note for diesel only combustion is that the two distinct stages of premixed combustion and diffusion-controlled burning can be clearly distinguished from the heat release rate curve (the latter stage commencing at about 9 CAD). Whereas, in the case of the CH_4-CO_2-H_2 mixture combustion, the heat release curve appears as a prolonged premixed stage. This is because the aspirated CH_4-CO_2-H_2 mixture can be assumed to be mixed almost homogenously with the intake air, and burns gradually with multiple flame propagation fronts which have been pilot ignited by the diesel fuel.

Fig. 7 shows that the peak heat release rate for diesel only combustion occurs at about 4 CAD ATDC. When the engine is run on the $80CH_4:20CO_2$ mixture, the peak heat release occurs at about 9 CAD ATDC (both with and without H_2). Increasing the proportion of CO_2 in the intake charge, that is, using the $60CH_4:40CO_2$ mixture, further shifts the peak heat release rate away from TDC (to about 12 CAD ATDC). The addition of 15% H_2 to both the CH_4-CO_2 mixtures does not appreciably change the time of peak hear release rate, but does have a noticeable effect on the peak heat release rate, as can be observed in Fig. 7.

Now, considering the heat release rate curves for the two CH_4-CO_2 mixtures shown in Fig. 7, it can be seen that the rate of increase of heat release is higher for the $80CH_4:20CO_2$ mixture (compared to $60CH_4:40CO_2$) resulting in a slightly higher peak heat release rate, considerably closer to engine TDC. The CO_2 in the aspirated mixtures does not contribute to energy release in the combustion chamber, but rather absorbs energy from the combustion flame, significantly curtailing burning velocities [8]. This effect of CO_2 is therefore more apparent in aspirated mixtures with a higher proportion of CO_2. It is interesting to note that the inclusion of H_2 in the CH_4-CO_2 mixtures tends to increase the peak heat release rate slightly (though to a lesser degree than that by which the heat release rates are decreased by increasing the proportion of CO_2 in the aspirated mixture), which can be attributed to the H_2 burning at higher flame temperatures as compared to CH_4.
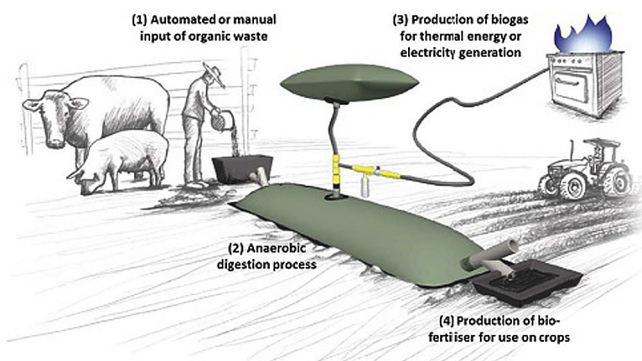
Fig. 8 shows the ignition delay period, time of peak heat release, peak heat release rates and the indicated thermal efficiency for the two pilot diesel fuel IMEPs of 0 bar and 1.5 bar, at a variety of engine loads and CH_4-CO_2-H_2 mixture proportions. The reader is reminded that the increase in engine load, above the pilot diesel fuel IMEP, was achieved by increasing amounts of CH_4-CO_2-H_2 mixtures supplied to the engine. For comparison purposes, Fig. 8 also shows the same parameters with diesel only combustion baseline tests, that is, without aspiration of any fuel gases. Ignition delay is defined here as the duration in CAD between the start of diesel fuel injection (SOI) and the start of combustion (SOC). SOI is taken to be the time when the actuation signal is sent to the injector, whereas the SOC is defined as the CAD of first detectable heat release following ignition.

It can be observed in Fig. 8 that the ignition delay period for both pilot diesel fuel IMEPs of 0 bar and 1.5 bar, and at all engine loads, is

Table 5
Test parameter matrix for biogas-diesel fuel co-combustion tests (*the balance was assumed to be made up of inert components and contaminants).

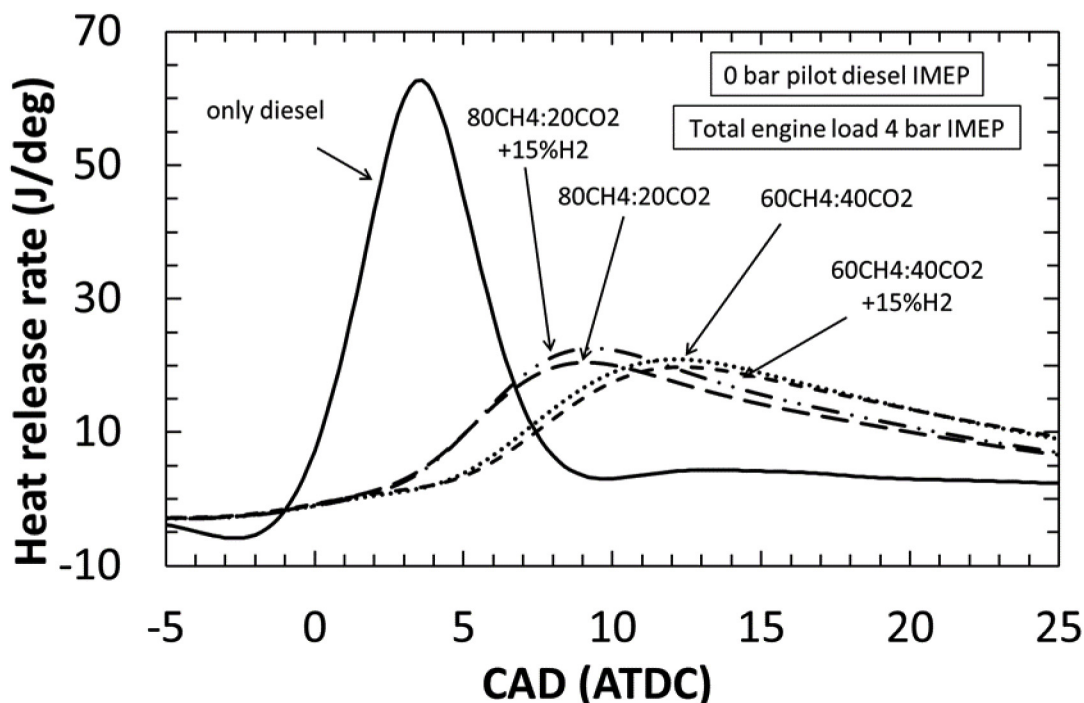| Sample name	$CH_4:CO_2$* mixture ratio (v/v)	Biogas flow rate (l/min)	Diesel fuel flow rate (ml/min)	Engine load (bar IMEP)
Biogas 1	$54CH_4:40.5CO_2$	4.6	6.5—12.7	3—7
Biogas 2	$48CH_4:29CO_2$	4.6	6.7—12.6	4—7

Fig. 6. Schematic of the commercial biodigester system, including feed stocks and use of outputs [36].

significantly higher for CH_4-CO_2-H_2 mixture combustion as compared to diesel only combustion baseline case. This can be explained, in general, by the reduction in local O_2 availability due to displacement of engine intake air by the aspirated CH_4-CO_2-H_2 mixtures. Comparing now the ignition delay period between the two pilot diesel fuel IMEPs, it can be seen from Fig. 8 that the ignition delay period is generally shorter for the higher quantity of pilot diesel fuel (that is, for 1.5 bar pilot diesel IMEP), probably due to the presence of a larger number of diesel ignition sites and thereby multiple flame propagation fronts, which promote CH_4-CO_2-H_2 mixture ignition. Finally, considering the effect on ignition delay period of adding H_2 to the two CH_4-CO_2 mixtures, it can be

seen from Fig. 8 that the ignition delay increases slightly and only for the 15% H_2 inclusion case, for both pilot diesel fuel IMEP conditions. The increase in ignition delay for low H_2 addition levels has also been previously observed in the case of H_2-diesel fuel co-combustion experiments [22]. This could possibly be attributed to the reduction in the O_2 concentration of the intake charge when some of the CH_4 was substituted, as shown in Table 2, by H_2 — the lower energy density of H_2 per unit volume results a greater displacement of engine intake air compared to CH_4 for the same engine load.

From Fig. 8 (c) and (d), it can be observed that the difference in the time of peak heat release rate (tPHRR) between $60CH_4:40CO_2$ and $80CH_4:20CO_2$ mixtures, at both pilot diesel IMEPs, is significantly more than the difference in the ignition delay period. Fig. 8 (e) and (f) shows that the peak heat release rates are lower for CH_4-CO_2-H_2 mixture combustion as compared to diesel only combustion, at both pilot diesel IMEPs and at all engine loads. This could be in part due to the in-cylinder CH_4-air and H_2-air mixtures being well below stoichiometric levels, and in part due to the energy absorbing effect of the inert CO_2.

Fig. 9 shows the indicated thermal efficiency and the exergetic efficiency for the various engine loads and CH_4-CO_2-H_2 mixtures. The indicated thermal efficiency of the engine shown in Fig. 9 (a) and (b) was calculated as the ratio of the indicated power output of the engine to the total energy input from diesel fuel, CH_4 and H_2. It can be observed that the thermal efficiencies are significantly lower for CH_4-CO_2-H_2 mixture combustion as compared to diesel-only combustion, at both pilot diesel IMEPs and at all engine loads. This could be attributed to the prolonged heat release rates and the

Fig. 7. Heat release rate curves for a pilot diesel fuel IMEP of 0 bar and various CH_4-CO_2-H_2 mixture proportions (v/v), at a constant engine load of 4 bar IMEP.
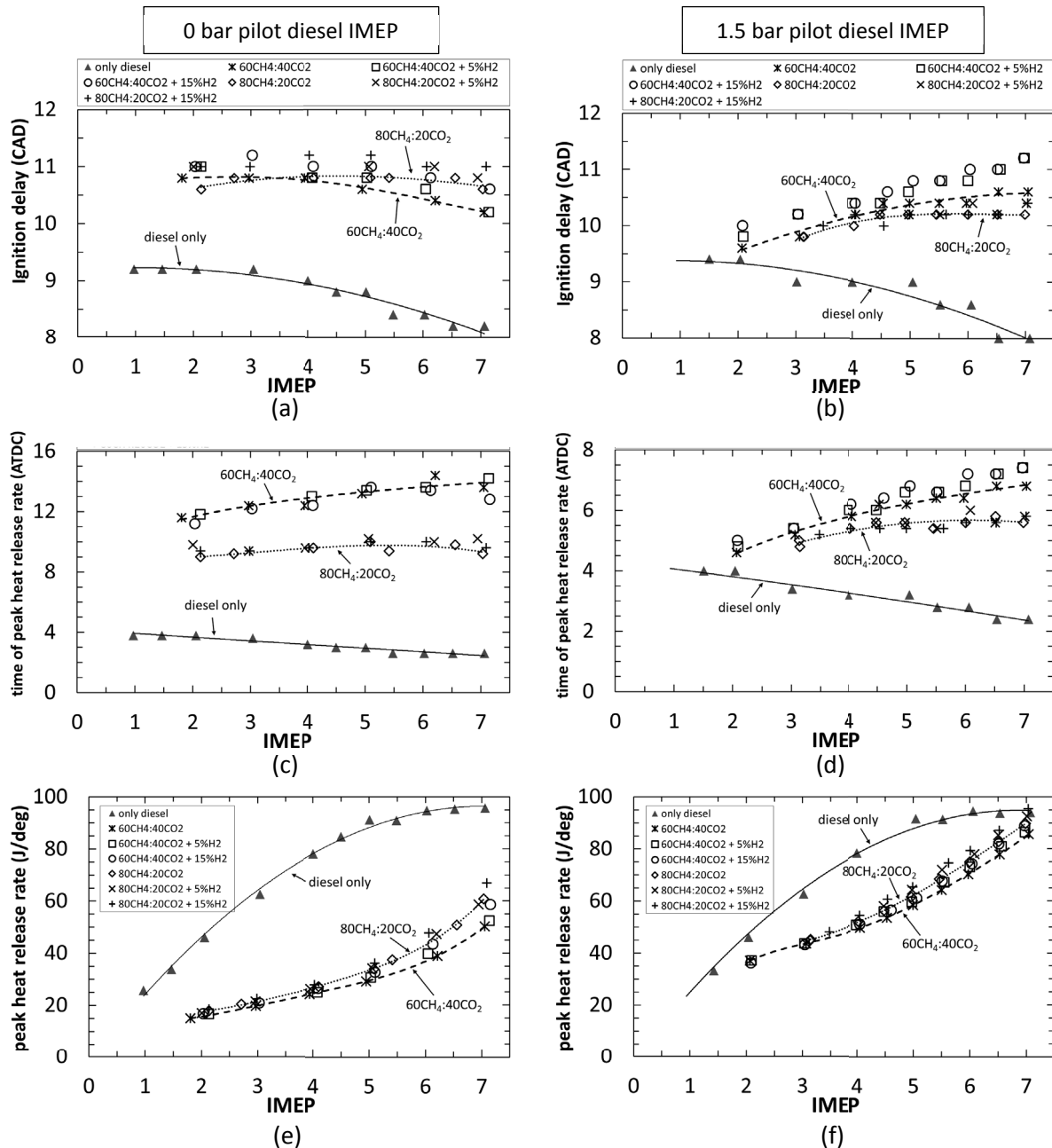
Fig. 8. Combustion characteristics for the two pilot diesel fuel IMEPs of 0 and 1.5 bar, at various engine loads and CH_4-CO_2-H_2 mixture proportions: (a) and (b) duration of ignition delay; (c) and (d) time of peak heat release rate; (e) and (f) peak heat release rates.

occurrence of peak heat release further away from the piston TDC position. The longer ignition delay will result in more energy being lost in the exhaust. However, preliminary calculations indicated that almost all the unburned THC emissions in the engine exhaust were due to the unreacted CH_4 persisting to the exhaust. Considering the 0 bar pilot diesel IMEP (Fig. 9(a)), the lowest efficiency is observed for the $60CH_4$:$40CO_2$ mixture which improves by about 1–1.5% with H_2 addition. This increase in thermal efficiency with the addition of H_2 could be expected, as the inert CO_2 was substituted by the more reactive H_2, which is more likely to increase combustion temperatures and help reduce the amount of unburned CH_4 lost in the exhaust. A further improvement (of about 1–2%) in thermal efficiencies is observed for the $80CH_4$:$20CO_2$ mixture (as compared to the $60CH_4$:$40CO_2$ mixture), which can be

attributed to the reduction of the inert CO_2 in the intake charge.

The exergy of a process is a measure of the difference between the net energy transfer through the system boundary and the energy destroyed within the system boundaries as a result of irreversibility [25,26]. The exergetic efficiency (Fig. 9 (c) and (d)) was calculated as the ratio between the exergy in the products to the total exergy input from the fuels, following the methodology initially established by Kotas [25], and further adapted for gaseous dual fuel co-combustion in diesel engines by various authors [26–31]. The exergy balance was determined by calculating the availability of energy in the fuel (diesel fuel and the CH_4-CO_2-H_2 mixtures), and its utilization in various ways including availability in shaft, cooling water, exhaust and destructed work [26]. The results in Fig. 9 (c) and (d) show that the exergetic efficiency follows a
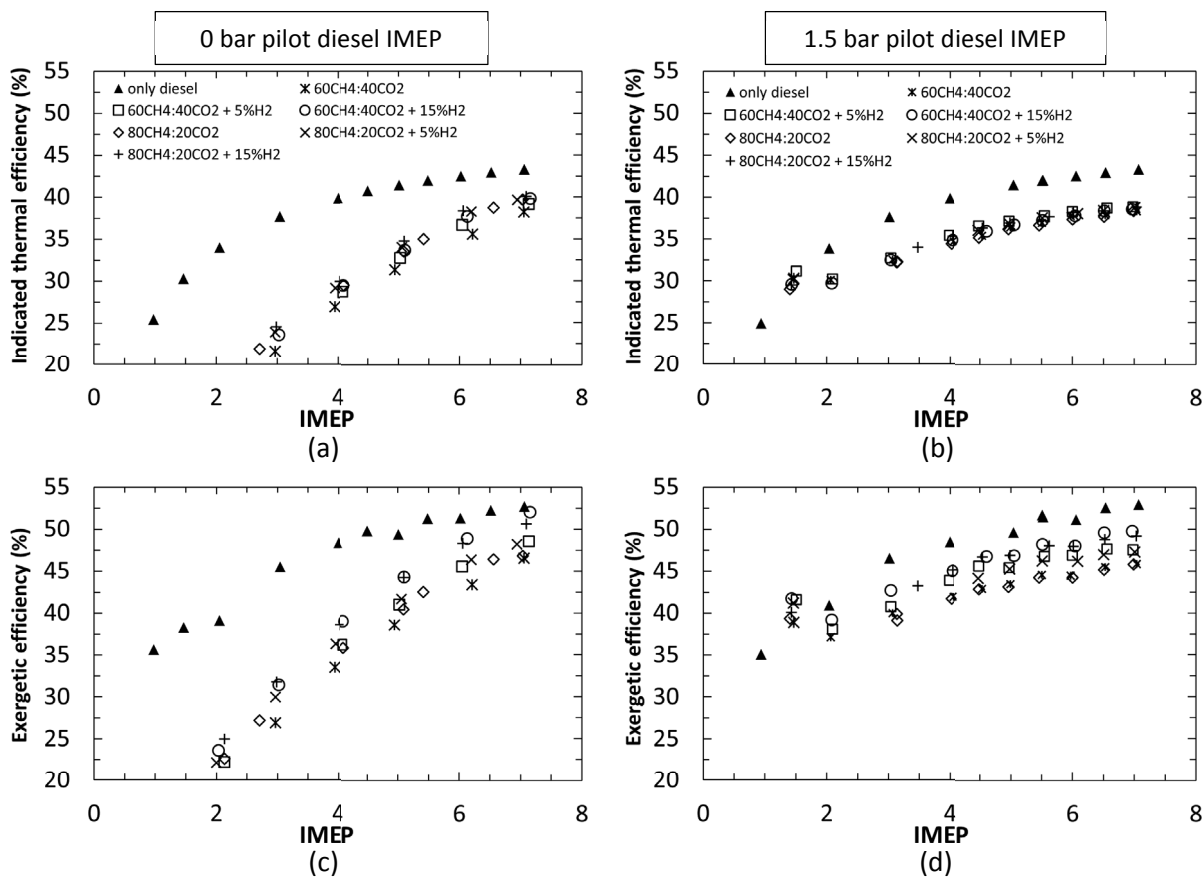
Fig. 9. (a) and (b) Indicated thermal efficiency, and (c) and (d) exergetic efficiency for the two pilot diesel fuel IMEPs of 0 and 1.5 bar, at various engine loads and CH_4-CO_2-H_2 mixture proportions.

similar trend as the indicated thermal efficiency, with the efficiency increasing at higher loads. The maximum exergetic efficiency is observed for the diesel only case at all engine loads; the drop in exergetic efficiency for the gas co-combustion cases might be due to the loss in available energy as a result of the intake fuel gas (CH_4-CO_2-H_2 mixtures) not burning completely inside the combustion chamber (that is, escaping unburned in the exhaust gases).

4.2. CO_2, NO_x and particulate exhaust emissions

Fig. 10 (a) and (b) show the gaseous exhaust emissions of CO_2 for the two pilot diesel fuel IMEPs of 0 bar and 1.5 bar, at various engine loads. For both pilot diesel fuel IMEPs of 0 and 1.5 bar and all CH_4-CO_2-H_2 mixtures, an almost linear increase in CO_2 emissions is observed as the quantity of the supplied CH_4-CO_2-H_2 mixture to the engine is increased in order to increase the engine load. Comparing the CO_2 emissions between the two CH_4-CO_2 mixtures, as would be expected, the CO_2 emissions from the $60CH_4$:$40CO_2$ mixture are higher due to the larger proportion of CO_2 in the aspirated mixture. Interestingly, it can also be observed from Fig. 10 (a) and (b) that CO_2 emissions from diesel only combustion are quite similar to CO_2 emissions from the $80CH_4$:$20CO_2$ mixture, that is, despite adding CO_2 in the aspirated mixture there is no increase in exhaust CO_2. Therefore, it can be assumed that the energy release from CH_4 results in less CO_2 production as compared to diesel combustion. A slight reduction in CO_2 emissions is observed, at both pilot diesel IMEPs and at all engine loads, when H_2 is included in the CH_4-CO_2 mixtures due to the H_2 displacing some of both CH_4 and CO_2.

Fig. 10 (c) and (d) show the gaseous exhaust emissions of NO_x for

the two pilot diesel fuel IMEPs of 0 bar and 1.5 bar, at various engine loads. Considering, first, the NO_x emissions for the pilot diesel fuel IMEP of 0 bar, it can be observed from Fig. 10 (c) that for engine loads below 4 bar IMEP the NO_x emission levels are below 100 ppm, in the case of CH_4-CO_2-H_2 mixtures. However, as the engine load increases above 4 bar IMEP, an almost exponential increase in NO_x emissions levels is observed. A probable explanation for these observations is as follows: at engine loads lower than 4 bar IMEP, the temperatures resulting from the combustion of the very lean in-cylinder CH_4-air and H_2-air mixtures (φ_{H2} = 0.018 and φ_{CH4} = 0.36 for the $80CH_4$:$20CO_2$+15% H_2 mixture at 4 bar IMEP engine load) were below the threshold temperatures (about 1000 K)) which promote rapid thermal NO_x formation. However, as the CH_4-CO_2-H_2 mixture being supplied to the engine was increased, in order to increase the engine load beyond 4 bar IMEP, the in-cylinder mixture concentration became sufficiently rich for the post combustion gas temperatures to go above the level at which NO_x formation rates accelerate significantly. This dependency of NO_x production rates on temperatures is a well-known phenomenon and is described by the extended Zeldovich mechanism [32]. Similar trends in NO_x emissions with increasing engine load can also be seen in Fig. 10 (d), however, an exponential rise in NO_x emissions occurs earlier, above about 2 bar IMEP. This is likely due to a higher quantity of diesel fuel being injected into the combustion chamber, corresponding to a pilot diesel IMEP of 1.5 bar.

The inclusion of H_2 in the CH_4-CO_2 mixtures does not appear to have a significant effect on NO_x emissions, except at the highest tested engine load condition of 7 bar IMEP. For example, at 7 bar
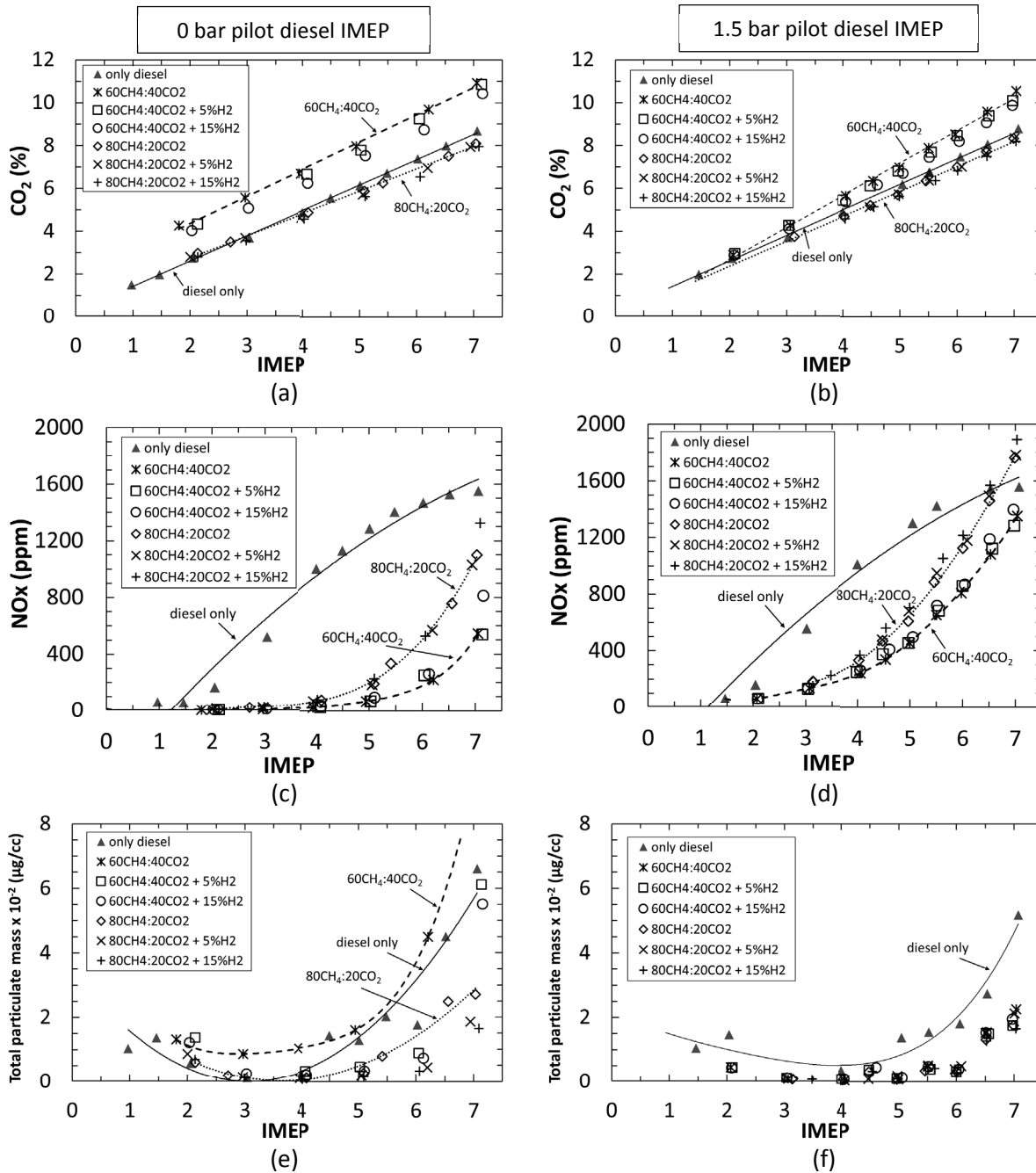
Fig. 10. Exhaust emissions of (a) and (b) carbon dioxide (CO_2), (c) and (d) oxides of nitrogen (NO_x) and (e) and (f) total particulate mass for the two pilot diesel fuel IMEPs, at various engine loads and CH_4-CO_2-H_2 mixture proportions.

IMEP (total engine load) and for a pilot diesel IMEP of 0 bar, the addition of 15% H_2 (v/v) to the 60CH_4:40CO_2 mixture increases NO_x emissions by almost 50%. This sharp increase in NO_x emissions at 7 bar IMEP is likely to have occurred due to the flame temperatures of the 60CH_4:40CO_2 + 15% H_2 mixture being considerably higher than those of the 60CH_4:40CO_2 mixture.

Fig. 10 (c) and (d) also show the NO_x exhaust emissions when the engine load is increased with diesel fuel only, that is, without any CH_4-CO_2-H_2 mixture addition. It can be seen that the NO_x emissions from CH_4-CO_2-H_2 mixture combustion, at nearly all engine loads, are lower than those from diesel only combustion. Inside the combustion chamber, the CH_4-CO_2-H_2 mixtures are both

locally and globally lean, which allows low temperature combustion, and hence reduced NO_x formation rates, while still maintaining diesel fuel comparable efficiencies [1,5]. In contrast, for diesel only fuelling (that is no CH_4-CO_2-H_2 mixture addition) the burning zone is naturally located where the diesel fuel-air mixture is approximately near stoichiometric, which results in high flame temperatures and high NO_x production rates.

Fig. 10 (e) and (f) show the exhaust emissions of total particulate mass (PM) for the two pilot diesel fuel IMEPs of 0 bar and 1.5 bar, at various engine loads. It can be observed that PM emissions increase sharply above engine loads of 5 bar IMEP (0 bar pilot diesel fuel IMEP) and 6 bar IMEP (1.5 bar pilot diesel fuel IMEP). This rapid

increase in PM emissions can also be seen to occur with diesel fuel only combustion (Fig. 10) and can be attributed to the increased diffusion-mode burn stage (more diesel fuel is injected) as the engine load increases beyond about 5 bar IMEP, and towards the highest tested load condition of 7 bar IMEP.

It can also be observed from Fig. 10 (e) that for a pilot diesel IMEP of 0 bar the PM emission levels for the $60CH_4:40CO_2$ mixture are significantly higher as compared to the $80CH_4:20CO_2$ mixture. It appears that the higher proportion of CO_2 in the $60CH_4:40CO_2$ mixture results in a greater level of O_2 displacement in the aspirated mixture as well as significant in-cylinder gas local temperature reduction due to thermal energy absorption, leading to reduced soot oxidation rates and higher PM emissions. The inclusion of H_2 to the $60CH_4:40CO_2$ mixture produces significant reductions in PM emissions, which could be attributed to two factors: reduction in fuel carbon supplied to the engine due to the displacement of some of the CH_4 by H_2, and higher post-combustion gas temperatures (and hence, increased soot oxidation rates) from CH_4-CO_2-H_2 mixtures, as compared to CH_4-CO_2 mixtures.

Comparing now Fig. 10 (e) and (f), it can be observed that the major difference in particulate emission levels between the two pilot diesel IMEPs of 0 and 1.5 bar, is only the higher particulate levels for the $60CH_4:40CO_2$ mixture. A likely reason for this can be the higher level of CO_2 in this aspirated mixture resulting in lower in-cylinder local flame temperatures. This suggestion is consistent with the observation discussed above that the addition of H_2 to the $60CH_4:40CO_2$ mixture reduces particulates, probably due to increased local flame temperatures as well as reduced rates of fuel carbon supplied to the engine. Another related observation from

Fig. 10 (e) is that the $60CH_4:40CO_2$ mixture results in particulate levels above those for diesel fuel only which is also likely to be due to the local flame temperatures, and hence soot oxidation rates, being suppressed by the higher level of CO_2 in the $60CH_4:40CO_2$ mixture.

4.3. In-cylinder gas sample composition

Fig. 11 shows the CO_2 concentration, at various engine loads, in gas samples extracted from the engine cylinder during sampling windows centred at 10, 25 and 40 CAD ATDC within the combustion cycle, with the two in-cylinder sampling arrangements relative to the diesel fuel sprays (Fig. 5). The tests were conducted for a fixed pilot diesel fuel IMEP of 1.5 bar and the increase in engine load was achieved by increasing the supply of the CH_4-CO_2-H_2 mixture to the engine. First, considering the $60CH_4:40CO_2$ mixture, it can be observed that the CO_2 concentrations in the sample are approximately equivalent for the two sampling arrangements, at all three sampling windows. This indicates that comparable quantities of CO_2 were generated in the region of the spray core and between the two sprays. In the region between the two sprays there is a lower concentration ('lack') of diesel fuel but plentiful air (along with the aspirated CH_4-CO_2-H_2 mixture), while in the region of the spray plume there is a lower concentration of air (and the CH_4-CO_2-H_2 mixture) but abundant diesel fuel. This results in similar amounts of air fuel mixture being consumed in both regions, and hence equivalent amounts of CO_2 detected in the gas samples collected from both regions.

The inclusion of 15% H_2 (v/v) to the $60CH_4:40CO_2$ mixture does not appear to have a significant effect on the in-cylinder CO_2
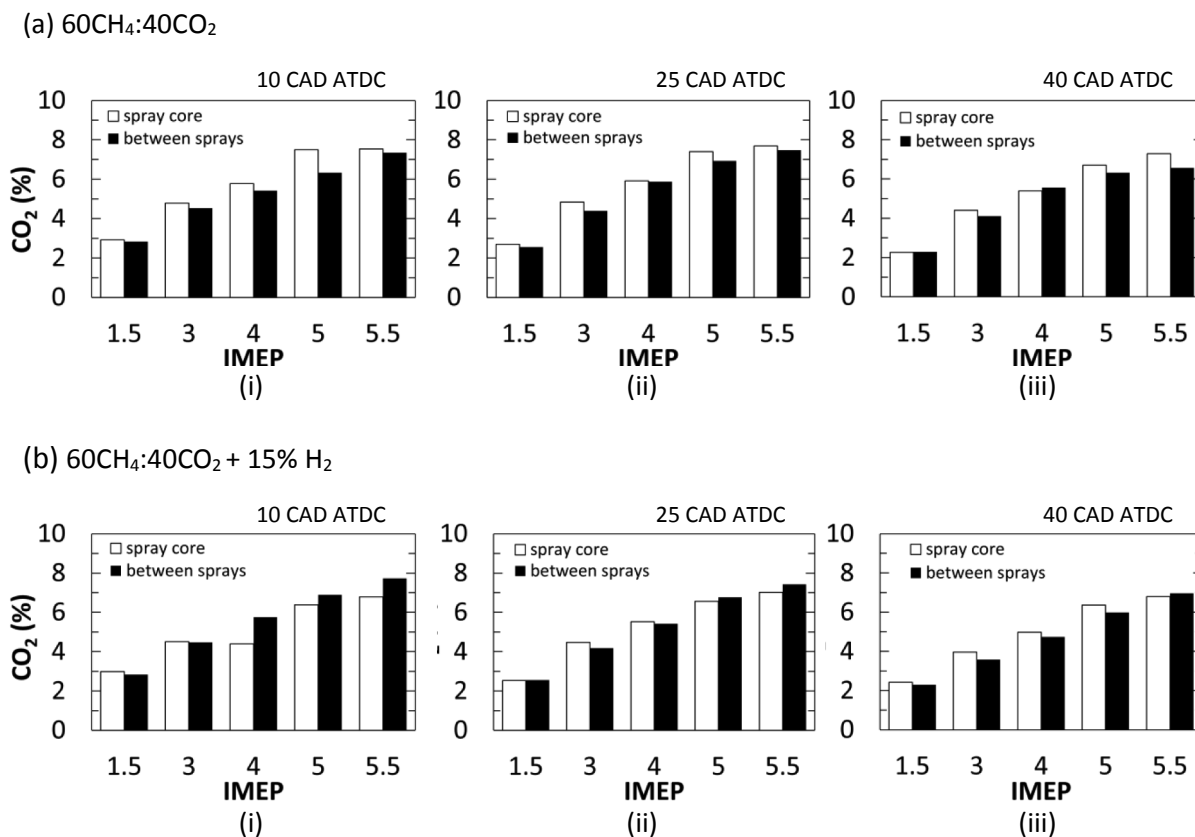
(a) $60CH_4:40CO_2$

(b) $60CH_4:40CO_2 + 15\% H_2$

Fig. 11. Measurement of carbon dioxide (CO_2) concentration for (a) $60CH_4:40CO_2$ and (b) $60CH_4:40CO_2 + 15\% H_2$ mixtures in in-cylinder gas samples collected at (i) 10 CAD, (ii) 25 CAD and (iii) 40 CAD ATDC at a fixed pilot diesel fuel IMEP of 1.5 bar with variable engine loads with two sampling arrangements (Fig. 5).

concentration, except for a slight increase in CO_2 levels in the region between the two sprays especially at 10 CAD and 25 CAD ATDC. This is most likely due to increased hydrocarbon oxidation rates as a result of increased flame temperatures for the CH_4-CO_2-H_2 mixture, as compared to the CH_4-CO_2 mixture.

Fig. 12 shows the unburned THC concentration, at various engine loads, in gas samples extracted from the engine cylinder at 10, 25 and 40 CAD ATDC of the combustion cycle with the two in-cylinder sampling arrangements. For both mixtures ($60CH_4$:$40CO_2$ and $60CH_4$:$40CO_2 + 15\% H_2$) it can be observed that the unburned THC concentrations at 10 CAD ATDC corresponding to the spray core region were higher than within the region between the fuel sprays. It could be assumed that at 10 CAD ATDC the diesel fuel spray has not fully broken down, and this is reflected in the high levels of unburned THC in the spray core region. In addition, the spray core region contains entrained CH_4 from the aspirated mixture, which appears as high levels of THC in the extracted gas samples. As the combustion cycle progresses from 10 to 25 CAD ATDC, the unburned THC levels in the spray core region are observed to decrease and approach THC levels similar to those in the region between the sprays (especially at high loads). This suggests that as combustion progresses, the spray core breaks down, and the subsequent mixing and combustion of diesel fuel and CH_4 with air results in lowers unburned THC levels. A final observation from Fig. 12 is that the addition of H_2 to the aspirated mixture brings a significant reduction in THC levels for both sampling arrangements, and this is likely to be due to higher local temperatures and enhanced combustion rates due to the presence of H_2.

Fig. 13 shows the NO_x concentration, at various engine loads, in gas samples extracted from the engine cylinder at sampling windows centred at 10, 25 and 40 CAD ATDC of the combustion cycle with the two in-cylinder sampling arrangements. First, considering the gas samples collected from the cylinder at 10 CAD and 25 CAD ATDC, it can be observed that NO_x levels are significantly higher in the region between the two sprays for the $60CH_4$:$40CO_2 + 15\% H_2$ mixture, as compared to the $60CH_4$:$40CO_2$ mixture. As suggested previously in this paper, the temperatures resulting from the combustion of the combined CH_4-H_2-air mixture are expected to be higher than those resulting from CH_4-air combustion, increasing NO_x formation rates. Now comparing the difference in NO_x concentrations between the two sampling arrangements, in the case of the $60CH_4$:$40CO_2 + 15\% H_2$ mixture, NO_x levels are higher in the region between the two sprays as compared to within the spray core region, especially at 10 CAD and 25 CAD ATDC. It would appear that the region between the two sprays benefits from the higher availability of air and gaseous fuel mixture, especially during the early stages of combustion when the spray core is yet to break down. This results in higher post combustion gas temperatures and, therefore, higher NO_x formation rates. On the other hand, the lower NO_x concentrations in the spray core region (at 10 CAD ATDC) implies a relatively low concentration of air in the fuel rich core of the diesel fuel spray, leading to lower combustion temperatures and reduced NO_x formation.

As combustion progresses from 10 to 25 CAD ATDC, NO_x levels are seen to increase in both regions, within spray core and between two sprays. It is likely that at 25 CAD ATDC, the rich diesel spay core
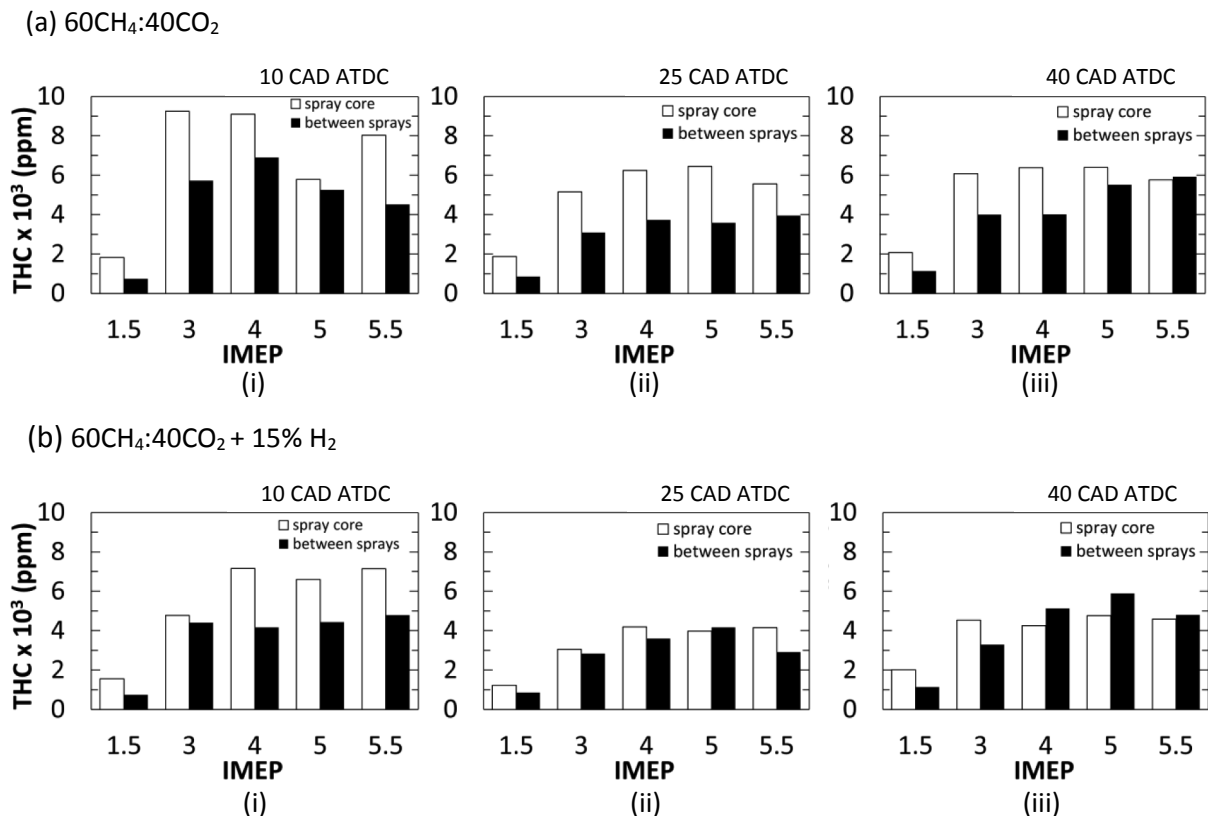

Fig. 12. Measurement of total unburned hydrocarbon (THC) concentration for (a) $60CH_4$:$40CO_2$ and (b) $60CH_4$:$40CO_2 + 15\% H_2$ mixtures in in-cylinder gas samples collected at (i) 10 CAD, (ii) 25 CAD and (iii) 40 CAD ATDC at a fixed pilot diesel fuel IMEP of 1.5 bar with variable engine loads with two sampling arrangements (Fig. 5).
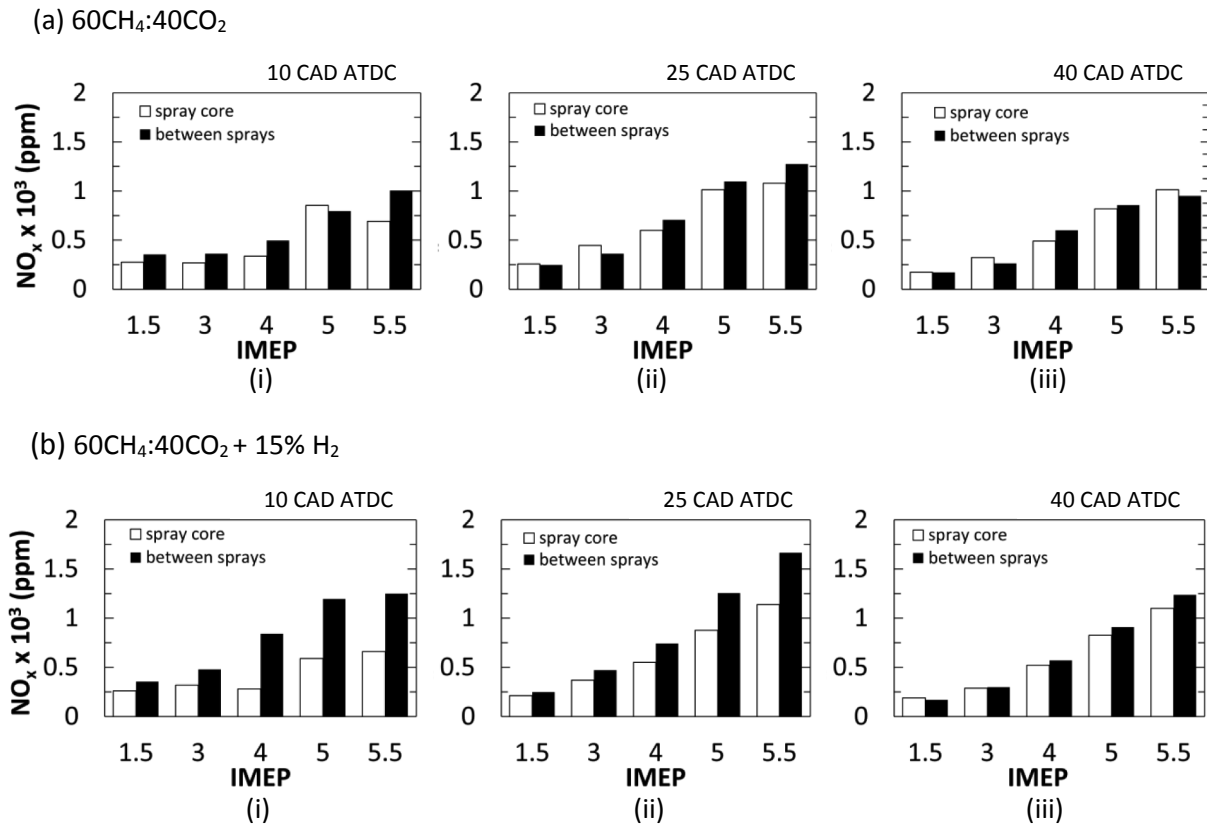
(a) $60CH_4:40CO_2$

(b) $60CH_4:40CO_2 + 15\% H_2$

Fig. 13. Measurement of nitrogen oxides (NO_x) concentration for (a) $60CH_4:40CO_2$ and (b) $60CH_4:40CO_2 + 15\% H_2$ mixtures in in-cylinder gas samples collected at (i) 10 CAD, (ii) 25 CAD and (iii) 40 CAD ATDC at a fixed pilot diesel fuel IMEP of 1.5 bar with variable engine loads with two sampling arrangements (Fig. 5).

was breaking down and entraining air and gaseous fuels, with the resulting air-fuel mixture burning at sufficiently high temperatures to raise NO_x formation rates. Beyond 25 CAD ATDC, the expansion of post combustion gases reduces temperatures significantly and NO_x equilibrium concentrations adjust to lower levels through reversible dissociation reactions, which is reflected in Fig. 13. At 40 CAD ATDC, NO_x levels become quite similar between the two sampling regions, for both the aspirated mixtures (Fig. 13 (iii)). This points towards a shift towards greater homogeneity in the contents of the highly turbulent engine cylinder during the expansion process, brought about by the combined effects of air swirl and reverse squish flow [33,34].

4.4. Exhaust emissions from real biogas

Fig. 14 shows the exhaust emissions of CO_2, CO, unburned THC, particulates and NO_x from the combustion of two real biogas samples of different CH_4-CO_2 compositions at various engine loads. The composition of biogas sample 1 was measured to be $54CH_4:40.5CO_2$, while that of biogas sample 2 was measured to be $48CH_4:29CO_2$; the balance for both biogas samples was assumed to be made up of components such as N_2 and H_2S. As the volumes of these biogas samples were quite limited, a different test procedure was employed for these tests as compared to that utilised so far in this paper. For these tests with real biogas, the flow rate of the biogas to the engine was kept fixed, and the increase in engine load was achieved by increasing the diesel fuel injection duration period (that is, the diesel fuel flow rate to the engine). For comparison

purposes, the exhaust emissions for diesel only combustion (no biogas addition) at equivalent engine loads have also been included.

It can be observed from Fig. 14 (a) that the CO_2 emissions from the two different biogas samples are only slightly higher than those for diesel only CO_2 emissions, at all loads up to 7 bar IMEP. The emissions of CO and unburned THC were generally higher for biogas sample 1 at all engine loads, as compared to both biogas sample 2 and diesel only condition (Fig. 14 (b) and (c)). This is likely to be due to the higher proportion of inert CO_2 in biogas sample 1 which could be expected to have caused a reduction in in-cylinder gas temperatures (by absorbing thermal energy), thereby curtailing oxidation rates of both CH_4 and diesel fuel and resulting in increased unburned (not ignited) or partially oxidised hydrocarbon emissions. Similarly, particulate emissions (Fig. 14 (d)) appeared to be higher for biogas sample 1 at all engine loads up to 5.5 bar IMEP, as compared to both biogas sample 2 and the diesel-only case, most likely due to the effect of reduced soot oxidation rates, as in the case of CO and unburned THC emissions. Above 5.5 bar IMEP, particulate emissions were observed to increase rapidly for both biogas samples and diesel only combustion, with the sharpest increase occurring for biogas sample 2. The sharp increase in PM emissions at engine loads above 5.5 bar IMEP could be attributed to the high amounts of diesel fuel being injected into the cylinder, resulting in a longer diffusion burn combustion stage. Now considering NO_x emissions, it can be observed from Fig. 14 (e), that NO_x emissions were lowest for biogas sample 1, as compared to both biogas sample 2 and diesel-only case. As mentioned before, the higher
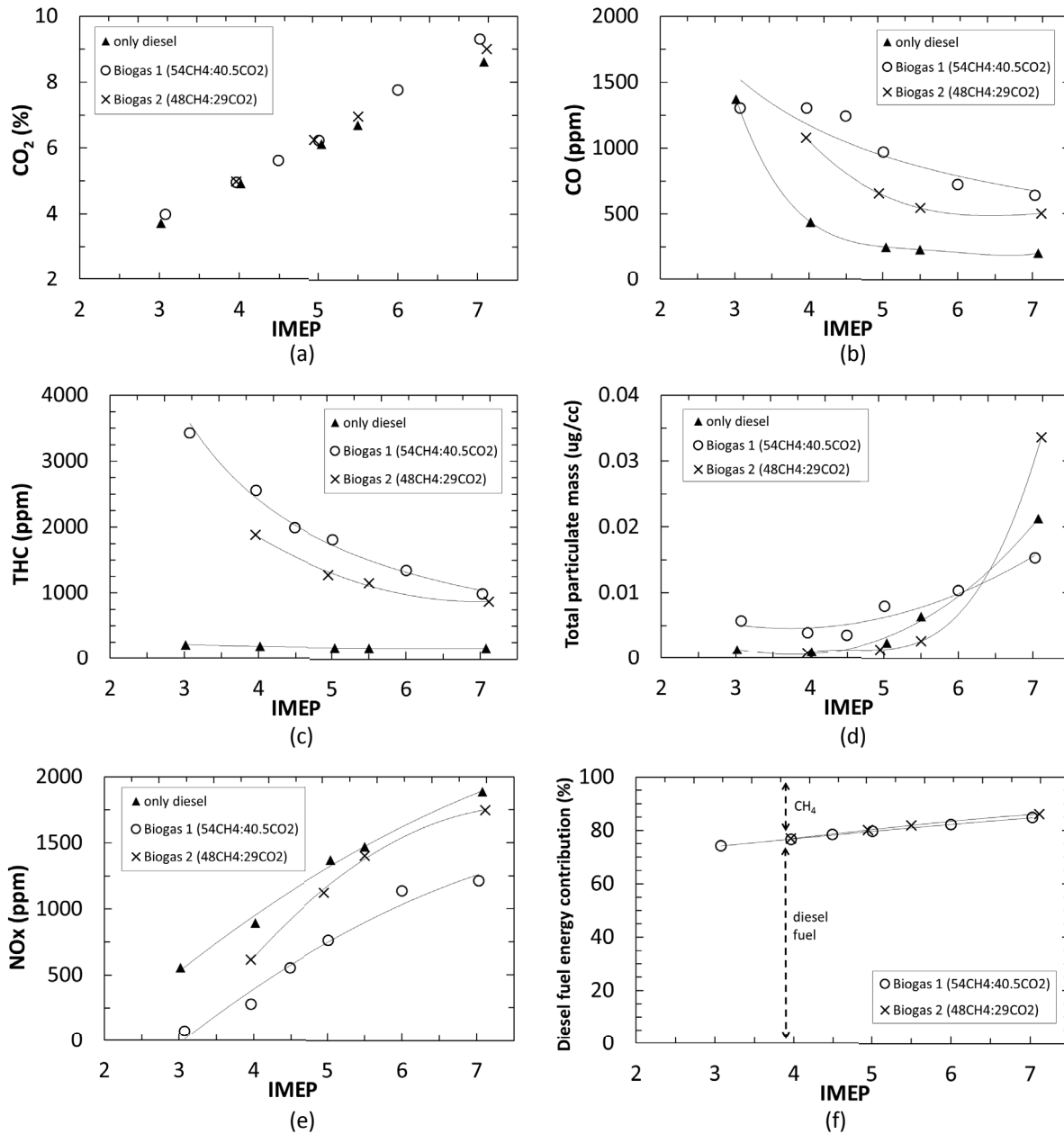
Fig. 14. Exhaust emissions of (a) CO_2, (b) CO, (c) unburned THC, (d) particulates and (e) NO_x for two real biogas samples for a fixed flow rate of biogas to the engine and various diesel fuel flow rates. For comparison, the exhaust emissions from diesel fuel only engine operation (no biogas addition) are also shown; (f) shows the percentage energy contribution of diesel fuel and CH_4 supplied to the engine at various engine loads.

proportion of CO_2 in biogas sample 1 (40.5% compared to 29% for sample 2) tends to lower in-cylinder gas temperatures, and since NO_x is produced primarily via high temperature augmented reactions [32,35], a reduction in in-cylinder gas temperatures can be expected to reduce NO_x formation rates.

A series of quick tests were conducted whereby the engine was instead supplied with simulated biogas mixed using compressed CH_4 and CO_2 gas bottles, of equivalent proportions to those of the real biogas samples tested. The purpose of these tests was to understand the effect of contaminants in the real biogas samples on the engine exhaust emissions. The results showed similar exhaust emission levels from the simulated biogas to those obtained from the real biogas samples, leading to the suggestion that the contaminants in the biogas sample do not have an adverse effect on

exhaust emissions.

5. Conclusions

1. The increase in heat release for the CH_4-CO_2-H_2 mixtures, pilot-ignited by diesel fuel, was considerably slower when compared to diesel fuel only combustion, resulting in lower peak heat release occurring relatively further away (later) from engine TDC. Peak heat release rates were observed to be lower for the $60CH_4$:$40CO_2$ mixture as compared to the $80CH_4$:$20CO_2$ mixture, at both pilot diesel IMEPs and at all engine loads. This was attributed to the presence of a higher proportion of CO_2 in the aspirated mixture impeding combustion through dilution of the combustible mixture and lower flame temperatures.

2. For a pilot diesel fuel IMEP of 1.5 bar, the ignition delay period was longer for the $60CH_4{:}40CO_2$ mixture, as compared to $80CH_4{:}20CH_4$ mixture, which was attributed to the higher proportion of inert CO_2 reducing rates of low temperature fuel breakdown reactions.

3. Exhaust CO_2 emissions were observed to be lower for diesel only combustion relative to the $60CH_4{:}40CO_2$ mixture, but equivalent to CO_2 emission from the $80CH_4{:}20CO_2$ mixture. This result underlines the desirability to scrub the biogas post-production so as to reduce its CO_2 content.

4. For both fixed pilot diesel IMEPs, NO_x emissions were observed to increase rapidly when the in-cylinder gas temperatures exceeded the threshold for NO_x formation temperatures. The thermal energy absorbing effect of the inert CO_2 resulted in NO_x emission from the $60CH_4{:}40CO_2$ mixture being lower as compared to the $80CH_4{:}20CO_2$ mixture.

5. Exhaust PM emissions for the $60CH_4{:}40CO_2$ mixture were observed to be greater as compared to both the $80CH_4{:}20CO_2$ mixture and the diesel-only case. The inclusion of H_2 to $60CH_4{:}40CO_2$ mixture significantly reduced PM emissions, suggested to be due to higher flame temperatures.

6. In-cylinder unburned THC levels at 10 CAD ATDC were observed to be higher in gas samples collected from within the spray core region, as compared to the region between two sprays. As the cycle progressed from 10 to 25 CAD ATDC and the diesel fuel spray core disintegrated due to air entrainment, the unburned THC levels in the spray core region were observed to decrease. In-cylinder NO_x levels were observed to be significantly higher in the region between two sprays for the $60CH_4{:}40CO_2 + 15\%\ H_2$ mixture, as compared to the $60CH_4{:}40CO_2$ mixture. It was suggested that this was a result of the temperatures from the CH_4-H_2-air mixture combustion being higher than those achieved by only CH_4-air combustion, resulting in higher NO_x formation rates.

7. Exhaust emissions from real biogas samples were in agreement with the trends obtained with the simulated CH_4-CO_2 mixtures. The CO_2 in the real biogas considerably reduced in-cylinder gas temperatures which lowered NO_x emissions, but at the same time increased CO, unburned THC and PM emissions due to reduced thermal oxidation rates.

Acknowledgements

Nomenclature

ATDC	after-top-dead-centre
BTDC	before-top-dead-centre
CAD	crank angle degree
CH_4	methane
CI	compression ignition
CO	carbon monoxide
CO_2	carbon dioxide
H_2	hydrogen
IMEP	indicated mean effective pressures
NO_x	nitrogen oxides
O_2	oxygen
PM	particulate mass
ppm	parts per million
rpm	revolutions per minute
SOC	start of combustion
SOI	start of injection
TDC	top -dead -centre
THC	total hydrocarbons
φ_{CH4}	methane-air equivalence ratio
φ_{H2}	hydrogen-air equivalence ratio

References

[1] Bora BJ, Saha UK, Chatterjee S, Veer V. Effect of compression ratio on performance, combustion and emission characteristics of a dual fuel diesel engine run on raw biogas. Energy Convers Manag 2014;87:1000–9. http://dx.doi.org/10.1016/j.enconman.2014.07.080.

[2] Yang L, Ge X, Wan C, Yu F, Li Y. Progress and perspectives in converting biogas to transportation fuels. Renew Sustain Energy Rev 2014;40:1133–52. http://dx.doi.org/10.1016/j.rser.2014.08.008.

[3] Tricase C, Lombardi M. State of the art and prospects of Italian biogas production from animal sewage: technical-economic considerations. Renew Energy 2009;34:477–85. http://dx.doi.org/10.1016/j.renene.2008.06.013.

[4] Sahoo BB, Sahoo N, Saha UK. Effect of engine parameters and type of gaseous fuel on the performance of dual-fuel gas diesel engines—a critical review. Renew Sustain Energy Rev 2009;13:1151–84. http://dx.doi.org/10.1016/j.rser.2008.08.003.

[5] Yoon SH, Lee CS. Experimental investigation on the combustion and exhaust emission characteristics of biogas-biodiesel dual-fuel combustion in a CI engine. Fuel Process Technol 2011;92:992–1000. http://dx.doi.org/10.1016/j.fuproc.2010.12.021.

[6] Mohamed Ibrahim M, Varuna Narasimhan J, Ramesh A. Comparison of the predominantly premixed charge compression ignition and the dual fuel modes of operation with biogas and diesel as fuels. Energy 2015;89:990–1000. http://dx.doi.org/10.1016/j.energy.2015.06.033.

[7] Jung C, Park J, Song S. Performance and NOx emissions of a biogas-fueled turbocharged internal combustion engine. Energy 2015;86:186–95. http://dx.doi.org/10.1016/j.energy.2015.03.122.

[8] Bari S. Effect of carbon dioxide on the performance of biogas/diesel duel-fuel engine. Renew Energy 1996;9:1007–10. http://dx.doi.org/10.1016/0960-1481(96)88450-3.

[9] Bedoya ID, Arrieta AA, Cadavid FJ. Effects of mixing system and pilot fuel quality on diesel-biogas dual fuel engine performance. Bioresour Technol 2009;100:6624–9. http://dx.doi.org/10.1016/j.biortech.2009.07.052.

[10] Barik D, Murugan S. Investigation on combustion performance and emission characteristics of a DI (direct injection) diesel engine fueled with biogas-diesel in dual fuel mode. Energy 2014;72:760–71. http://dx.doi.org/10.1016/j.energy.2014.05.106.

[11] Makareviciene V, Sendzikiene E, Pukalskas S, Rimkus A, Vegneris R. Performance and emission characteristics of biogas used in diesel engine operation. Energy Convers Manag 2013;75:224–33. http://dx.doi.org/10.1016/j.enconman.2013.06.012.

[12] Henham A, Makkar M. Combustion of simulated biogas in a dual-fuel diesel engine. Energy Convers Manag 1998;39:2001–9. http://dx.doi.org/10.1016/S0196-8904(98)00071-5.

[13] Mustafi NN, Raine RR, Verhelst S. Combustion and emissions characteristics of a dual fuel engine operated on alternative gaseous fuels. Fuel 2013;109:669–78. http://dx.doi.org/10.1016/j.fuel.2013.03.007.

[14] Gunea C, Razavi MRM, Karim GA. The effects of pilot fuel quality on dual fuel engine ignition delay. SAE Pap; 1998. p. 982453. http://dx.doi.org/10.4271/982453.

[15] Agarwal A, Assanis DN. Multi-dimensional modeling of natural gas ignition under compression ignition conditions using detailed chemistry. SAE Pap; 1998. p. 980136. http://dx.doi.org/10.4271/980136.

[16] Stelmasiak Z. The impact of gas-air composition on combustion parameters of dual fuel engines fed CNG. SAE Pap; 2002. http://dx.doi.org/10.4271/2002-01-2235. 2002–01–2235.

[17] Cacua K, Amell A, Cadavid F. Effects of oxygen enriched air on the operation and performance of a diesel-biogas dual fuel engine. Biomass Bioenergy 2012;45:159–67. http://dx.doi.org/10.1016/j.biombioe.2012.06.003.

[18] Karim G. Hydrogen as a spark ignition engine fuel. Int J Hydrogen Energy 2003;56:256–63.

[19] Nagalingam B, Duebel F, Schmillen K. Performance study using natural gas, hydrogen-supplemented natural gas and hydrogen in AVL research engine. Int J Hydrogen Energy 1983;8:715–20. http://dx.doi.org/10.1016/0360-3199(83)90181-7.

[20] Lilik G, Zhang H, Herreros J. Hydrogen assisted diesel combustion. Int J Hydrogen Energy 2010;35:4382–98. http://dx.doi.org/10.1016/j.ijhydene.2010.01.105.

[21] Christodoulou F, Megaritis A. Experimental investigation of the effects of separate hydrogen and nitrogen addition on the emissions and combustion of a diesel engine. Int J Hydrogen Energy 2013;38:10126–40. http://dx.doi.org/10.1016/j.ijhydene.2013.05.173.

[22] Talibi M, Hellier P, Balachandran R, Ladommatos N. Effect of hydrogen-diesel fuel co-combustion on exhaust emissions with verification using an in–cylinder gas sampling technique. Int J Hydrogen Energy 2014;39:15088–102. http://dx.doi.org/10.1016/j.ijhydene.2014.07.039.

[23] Talibi M, Hellier P, Balachandran R, Ladommatos N. Development of a fast-acting, time-resolved gas sampling system for combustion and fuels analysis. SAE Int J Engines 2016;9. http://dx.doi.org/10.4271/2016-01-0791. 2016—01—0791.

[24] Saravanan N, Nagarajan G. An experimental investigation of hydrogen-enriched air induction in a diesel engine system. Int J Hydrogen Energy 2008;33:1769—75. http://dx.doi.org/10.1016/j.ijhydene.2007.12.065.

[25] Kotas TJ. The exergy method of thermal plant analysis. Melbourne, FL, United States: Krieger Publishing Company; 1995.

[26] Panigrahi N, Mohanty MK, Mishra SR, Mohanty RC. Performance, emission, energy, and exergy analysis of a C.I. Engine using mahua biodiesel blends with diesel. Int Sch Res Not 2014:1—13. http://dx.doi.org/10.1155/2014/207465.

[27] Özkan MA. Comparative study on energy and exergy analyses of a CI engine performed with different multiple injection strategies at Part Load: effect of injection pressure. Entropy 2015;17:244—63. http://dx.doi.org/10.3390/e17010244.

[28] Bourhis G, Leduc P. Energy and exergy balances for modern diesel and gasoline engines. Oil Gas Sci Technol — Rev l'Institut Français Du Pétrole 2010;65: 39—46. http://dx.doi.org/10.2516/ogst/2009051.

[29] Waller MG, Williams ED, Matteson SW, Trabold TA. Current and theoretical maximum well-to-wheels exergy efficiency of options to power vehicles with natural gas. Appl Energy 2014;127:55—63. http://dx.doi.org/10.1016/j.apenergy.2014.03.088.

[30] Chintala V, Subramanian KA. Assessment of maximum available work of a hydrogen fueled compression ignition engine using exergy analysis. Energy 2014;67:162—75. http://dx.doi.org/10.1016/j.energy.2014.01.094.

[31] Jafarmadar S. Exergy analysis of hydrogen/diesel combustion in a dual fuel engine using three-dimensional model. Int J Hydrogen Energy 2014;39: 9505—14. http://dx.doi.org/10.1016/j.ijhydene.2014.03.152.

[32] Miller JA, Bowman CTC. Mechanism and modeling of nitrogen chemistry in combustion. Prog Energy Combust Sci 1989;15:287—338. http://dx.doi.org/10.1016/0360-1285(89)90017-8.

[33] Heywood JB. Internal combustion engine fundamentals. first ed. New York: McGraw-Hill; 1988.

[34] Zhao H, Lowry G, Ladommatos N. Time-resolved measurements and analysis of in-cylinder gases and particulates in compression-ignition engines. SAE Pap; 1996. p. 961168. http://dx.doi.org/10.4271/961168.

[35] Bowman CT. Kinetics of nitric oxide formation incombustion processes. Symp Combust 1973;14:729—38. http://dx.doi.org/10.1016/S0082-0784(73)80068-2.

[36] Biobolsa. Sistema biobolsa anerobic digester. 2015 (accessed April 5, 2015), http://sistemabiobolsa.com/what-we-do/the-technology/.